THE JOURNAL OF PHYSICAL CHEMISTRY B

ARTICLE

pubs.acs.org/JPCB

Effects of Tether Length on the Behavior of Amphiphilic Bent-Core Molecules at Water Surfaces

Timothy J. Smith,[†] Wilder Iglesias,[‡] Sharon R. Stefanovic,[§] Elizabeth K. Mann,[§] Carsten Tschierske,[∥] Antal Jákli,[‡] and Daniel J. Lacks*[,†]

[†]Chemical Engineering, Case Western Reserve University, Cleveland, Ohio 44106, United States

[‡]Liquid Crystal Institute, Kent State University, Kent, Ohio 44242, United States

[§]Physics Department, Kent State University, Kent, Ohio 44242, United States

[∥]Institute of Organic Chemistry, Martin-Luther-University Halle-Wittenberg, Halle D06120, Germany

ABSTRACT: Alignment layers for bulk liquid crystalline phases can be created with monolayers formed by Langmuir−Schaefer techniques. Monolayer stability is a function of the propensity of the component molecule to effectively pack at a water interface; this propensity is enhanced when the molecule has an appropriate balance of hydrophilicity and hydrophobicity and the desired liquid crystalline order, as well as other structural factors. Our experiments show that molecules based on a bent-core with one hydrophilic and one hydrophobic end can form stable monolayers that act as effective alignment layers. However, the stable monolayers only form when the hydrophilic end has a sufficiently short chain. Molecular simulations carried out for both dilute concentrations (1 bent-core molecule) and high concentrations (25 bent-core molecules) on a water surface elucidate this behavior. The hydrophilic group acts to tether the molecule to the water surface, with a tether floppiness that depends on the tether length. At dilute concentrations, these molecules lay flat on the water surface (the molecular long axis approximately parallel to the surface), and the tether floppiness has little consequence. However, at high concentrations, the molecules pack with orientations approximately perpendicular to the surface; they stand upright on the tether, and the floppier tether leads to wobbly legs that cause large lateral fluctuations in the molecular positions and reduce monolayer stability.

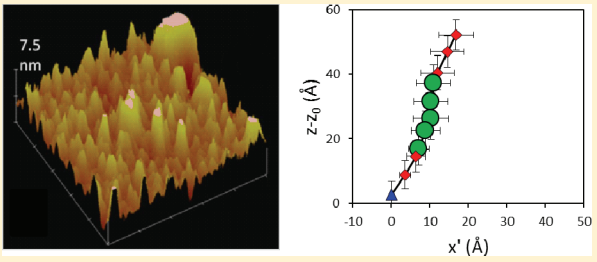

INTRODUCTION

Bent-core molecules exhibit a wide range of interesting properties and potential applications. These molecules can form many smectic phases, from B1−B8, which have prompted much research on the structure and behavior of the phases.[1,3] Bent-core molecules behave as non-Newtonian fluids that can (in some cases) form fibers[4] and have been used as side chains on polymers to form liquid crystal elastomers with rubber elasticity and smectic ordering.[5] The chirality[6] and polar switching of bent-core liquid crystals give rise to ferroelectricity within some smectic layers.[7,8] In addition, optically active systems of bent-core liquid crystals can be controlled by electric fields.[2] Applications have not yet exploited the potential of ferroelectric phases, due in part to the difficulty of aligning the bulk liquid crystals. This article addresses issues involved with the development of methods to carry out this alignment.

A bulk liquid crystal can be aligned by surface layers that guide the self-packing of the liquid crystal molecules at the interfaces, with this order transmitted from the interface into the bulk liquid crystal. Alignment layers have been ineffective for bent-core liquid crystals, probably because the usual alignment layers are incompatible with the shape and symmetry of the bent-core molecules.[9,10] For this reason, an alignment layer composed of bent-core molecules may be more effective. In this direction, we showed that a layer of bent-core molecules, formed as a Langmuir monolayer at the air/water interface and then transferred to a glass surface by Langmuir−Schaefer techniques, can align a bent-core nematic liquid crystal.[11] While the monolayers of bent-core molecules have been produced by several groups,[12−18] these monolayers were unstable under compression[11,15,19] and could only impart parallel alignment in the liquid crystal cell.[11,20,21] The reason for these limitations is that in these molecules the central core is hydrophilic, with hydrophobic pendent groups at both ends, which causes the molecules to lay horizontal on the water surface.

In order to produce films with vertical alignment and higher stability under compression, we introduced bent-core molecules that have a hydrophilic end to create a tether at the water surface. Films made with these molecules were indeed both more stable and, for the first time, produced a vertical alignment in a bent-core nematic liquid crystal.[9,10] From these results, we deduced that the hydrophilic end-group indeed acted as a tether.

Received: August 17, 2011
Revised: September 30, 2011
Published: October 04, 2011

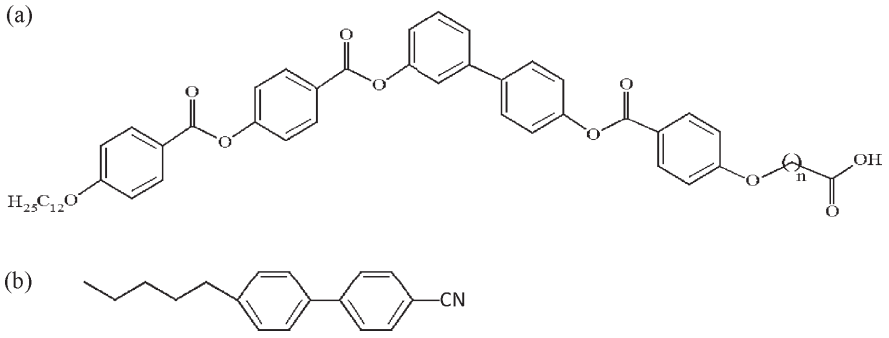

Figure 1. Chemical structure of (a) Z10 (n = 10) and Z4 (n = 4); (b) 5CB.

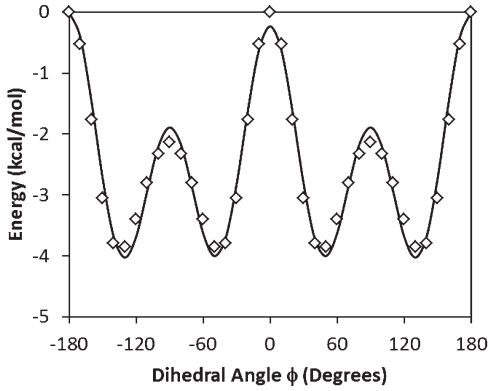

Figure 2. Potential energy in a biphenyl molecule as a function of interphenyl dihedral. The symbols are electronic structure results from Karpfen et. al,[27] and the solid line is the fitted function.

Here, we explore the action of the tether in more detail, with the goal of understanding how to create optimal alignment layers. We address the length of the relatively flexible hydrocarbon chain linking the hydrophilic end to the more rigid bent core. To do so, we compare the behavior of two bent-core molecules, shown in Figure 1, which have different tether lengths: Z10, with tether length n = 10, and Z4, with tether length n = 4 (note that in previous publications Z4 was called Z2b[10]).[22] This investigation is carried out with a combined experimental and simulation approach.

EXPERIMENTAL METHODS

The synthesis and purification of both bent-core molecules together with the analytical data and the investigation of the thermotropic LC behavior have been reported previously.[22] To create the monolayers, either Z10 or Z4 is dissolved in chloroform and spread on the top of pure water (PureLab Plus system; resistivity of 18.2 MΩ·cm and passes the shake test, meaning that small bubbles in solution burst as soon as they reach the surface) in a Langmuir trough. The KSV minitrough system is used to create a surface tension isotherm; control barriers moving at 2.5−5 mm/min are used to compress and decompress the system. The film is removed from the water and placed on a glass slide via inverse Langmuir−Schaefer (ILS) techniques. Atomic force microscopy (AFM, NanoScope III) is used in the tapping mode to generate images of the topography of these ILS films.[11]

We test the effectiveness of the ILS films as alignment layers for 5CB (Figure 1b), a simple rod-like nematic liquid crystal; the alignment of 5CB serves as an indicator of the orientation and uniformity of the underlying bent-core film.[23] An aligned 5CB liquid crystal cell is created between glass slides coated with either the Z10 or Z4 ILS monolayer. The alignment of the 5CB bulk liquid crystal, which is expected to correlate with the orientation of the hydrocarbon chains of the ILS monolayer, is determined via polarized optical microscopy (POM). In the POM procedure, the film cell is placed on a platform under an optical microscope between crossed polarizers. The platform is rotated until the dark state, with minimal light transmission, is reached (the dark state occurs when the cell director is aligned with the microscope polarizer or analyzer). The platform is then rotated 45° from the dark state to the light state, with maximum light transmission. The contrast between these dark and light states is a measure of the alignment of the film. A film with good alignment perpendicular to the surface is symmetric with respect to rotation and thus has low contrast, and a film with good alignment parallel to the surface has uniform dark and light states. In contrast, a film with poor alignment has a mixture of dark and light domains for any film orientation.

COMPUTATIONAL METHODS

Molecular dynamics simulations, which track the trajectory of atoms moving over time in response to the intermolecular forces, are used to elucidate the different behaviors of Z10 and Z4 bent-core molecules on water surfaces. In our simulations, each atom is explicitly modeled (rather than using larger pseudoatoms). The simulation cell includes ∼8000 atoms and has periodic boundary conditions in all three dimensions to remove surface effects (in the x- and y-dimensions). To create the water surface, the simulation cell is constructed with the z-dimesion much larger than the x- and y-dimensions, such that the water molecules form a two-dimensional slab perpendicular to the z-dimension.

The optimized potentials for liquid simulations (OPLS) force field[24] is used to model molecular interactions. All necessary parameters are included in the Gromacs package except for the following: (a) the ester oxygen bond angle bending interactions, which are taken from Charifson et al.,[25] and (b) the biphenyl dihedral interaction, which is obtained by fitting the Ryckaert−Bellemans function[26] $V(\phi) = \sum_{n=0}^{5} C_n[\cos(\phi - 180)]^n$ to the electronic structure results (obtained with the second-order Møller−Plesset method) for the energy of the biphenyl molecule as a function of the interphenyl dihedral angle.[27] In this fitting

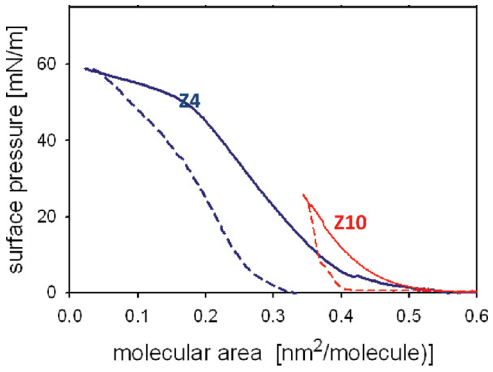

Figure 3. Isotherms for bent-core molecules: Z10 (thin red lines) and Z4 (thicker blue lines). Solid lines are results of compression, and dashed lines are results of decompression.

procedure, the parameters C_n were varied to fit the sum of $V(\phi)$ and the nonbonded energy (in calculating the nonbonded energy, all bond lengths and angles remained fixed as ϕ changed). The fitted energy is compared to the electronic structure energy in Figure 2; the small differences between the fit and the energy values are due to the limited variability inherent in the Ryckaert−Bellemans function.

The simulations are carried out for systems consisting of 2500 water molecules and either 1 or 25 bent-core molecules; the simulations with 1 molecule represent the infinite dilution limit, and the simulations with 25 molecules represent systems with surface areas of 0.23 nm^2/molecule. The simulation cell has *x*- and *y*-dimensions of 5.4 nm and a *z*-dimension of 12 nm; this choice of simulation cell dimensions leads to slabs of water approximately 2.7 nm thick, and the wide (>9 nm) vacuum layer separating the water slabs ensures that the interaction between slabs is negligible. The starting configuration consists of the annealed bent-core molecules placed in the vacuum layer between water slabs. All simulations are carried out at a temperature of 300 K.

The simulations are carried out for 35 ns, where the first 10 ns is used for equilibration, and data is collected in the final 25 ns. The molecular structures are analyzed in terms of probability distributions of the positions of different segments of the molecule. Along the *z*-dimension, these positions are compared to the position of the water surface, which is defined here as the Gibbs dividing surface.[28]

The molecular dynamics simulation details are as follows. The particle-mesh Ewald method[29] is used to calculate the Coulombic interactions, and a direct summation to a cutoff length of 1 nm is used to calculate the non-Coulombic interactions. A fixed temperature is maintained using a velocity rescaling thermostat[30] with a time constant of 1 ps; the thermostat is applied separately for the bent-core and water molecules to ensure the equilibration of energy. The time step used for the numerical integration of the equations of motion is 1 fs. The simulations are carried out with the Gromacs software package.[31]

The bent core molecules are initially annealed to ensure that they are not trapped in nonequilibrium configurations near the (arbitrary) starting configuration. The annealing is carried out for the molecule in a vacuum, with a series of 100 ps simulations; the simulations begin at $T = 1000$ K, and each subsequent simulation is run at a temperature lowered by 100 K, down to $T = 300$ K.

EXPERIMENTAL RESULTS

The surface pressure isotherms for Z10 and Z4 are shown in Figure 3. For both molecules, the surface pressure starts rising when the molecular area (i.e., area/molecule) is ∼0.5 nm^2, which corresponds to a film thickness of ∼3 nm (estimated assuming the bulk film density). The films collapse at pressures of 20−60 mN/m. When the films are decompressed after collapse, the films respread such that a viscoelastic monolayer covers the surface after decompression to zero pressure.[32] This behavior is not common for films of bent-core molecules with two hydrophobic ends; for films composed of these molecules, the surface pressure starts rising at a much smaller molecular area, and the films do not respread upon decompression.[9−11,15] In comparing films composed of Z10 and Z4, it is seen that the shorter tether allows the molecules to be more highly compressed in a monolayer and sustain higher pressures.

AFM results, shown in Figure 4, display significant differences for ILS films composed of Z10 and Z4 molecules. In particular, while the root mean squared height deviations R_q are roughly the same for the two molecules at similar surface pressures (at surface pressure $\pi \approx 8$ mN/m, R_q =1.8 nm for Z10 and 2.1 nm for Z4; and at $\pi \approx 20$ mN/m, R_q =4.3 nm for both Z4 and Z10), the horizontal scale or correlation length of these height variations is almost an order of magnitude larger for Z10 (∼100 nm) than for Z4 (∼20 nm) films. Thus, the longer tether in Z10 seems to lead to a more gradual change in film thickness. The AFM image for Z10 at low pressure, Figure 4a, shows a ring formation. Such ring formations have been seen in films of many different types of molecules.[33−36] The closest analogy is the similar structures previously reported by Liu et al. with a very different bent-core molecule at low pressures.[36] These authors conclude that the ring structures form when a bent-core molecule has a sufficiently long terminal chain, so the film has enough fluidity to have a nematic-like arrangement, which is disrupted by disclinations produced by the molecular shape, resulting in a spiral conformation. This type of self-assembly could contribute to the poor stability observed for Z10 monolayers.

The results of polarized microscopy on 5CB sandwiched between films of ILS monolayers are shown in Figure 5. The difference in the tether length clearly plays an important role in the alignment properties of these monolayers. For both Z10 and Z4 films, the 5CB cell is closer to the planar alignment for ILS films formed at low transfer pressures and closer to perpendicular alignment for ILS films formed at high transfer pressures. However, the alignment is much more uniform for Z4, the molecule with the shorter tether. This result correlates well with the more stable isotherms of Z4 and suggests that Z4 forms a more organized layer.

COMPUTATIONAL RESULTS

First, we compare the structures of the Z10 and Z4 molecules on the water surface in the infinite dilution limit (a single Z10 or Z4 molecule on the water surface). The distributions of the heights of various parts of the molecules relative to the water surface are shown in Figure 6b. The molecule essentially lays flat on the surface, but the lowest part of the molecule is the acid end, and the highest part of the molecule is the aliphatic end; the most probable height of the aliphatic end is approximately 3 Å above that of the acid end. While the structures of Z10 and Z4 are very similar in regard to the positions of the center and the end segments, Figure 6c shows that the alkyl chain connecting the

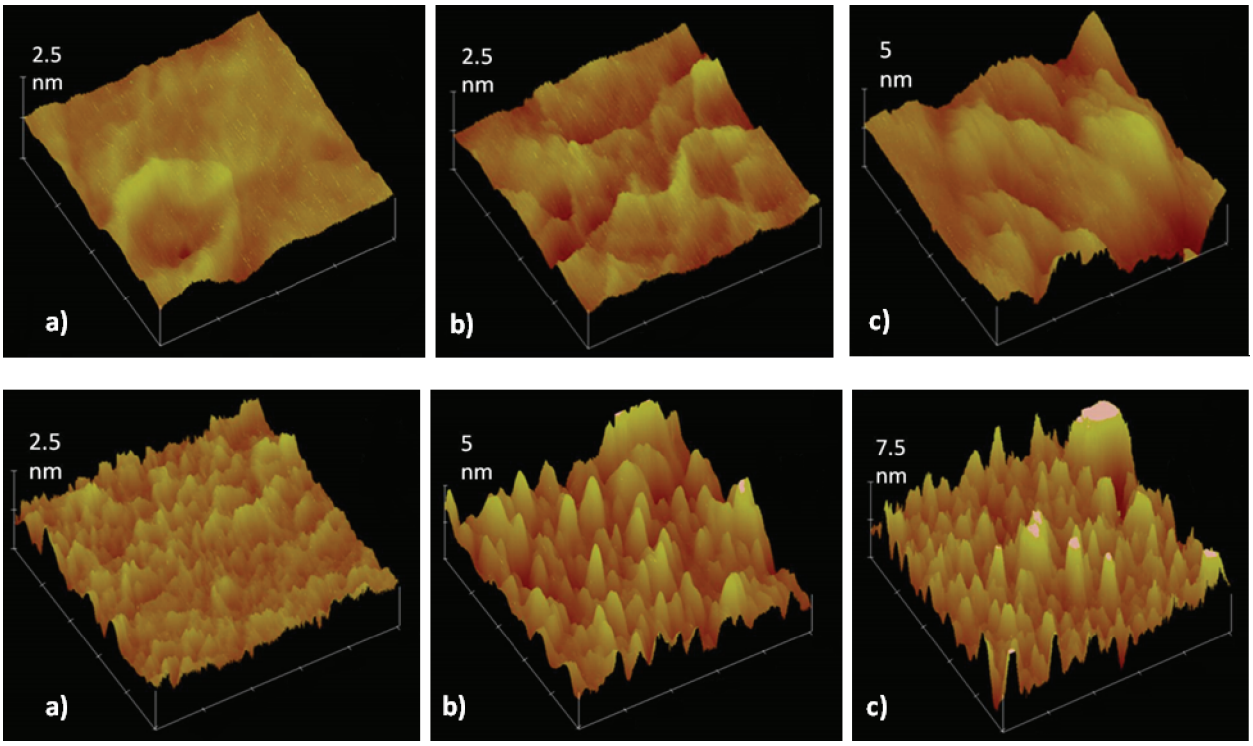

Figure 4. AFM pictures of ILS monolayer-coated glass slides transferred from a Langmuir trough at different surface pressure. The images are 500 nm × 500 nm horizontally. Top: Z10, (a) surface pressure $\pi = 2$ mN/m, mean squared deviation $R_q = 1.7$ nm; (b) $\pi = 8$ mN/m, $R_q = 1.8$ nm; (c) $\pi = 17$ mN/m, $R_q = 4.33$. Bottom: Z4, (a) $\pi = 8$ mN/m, $R_q = 2.2$ nm; (b) $\pi = 21$ mN/m, $R_q = 4.3$ nm; (c) $\pi = 33$ mN/m, $R_q = 6.5$ nm.

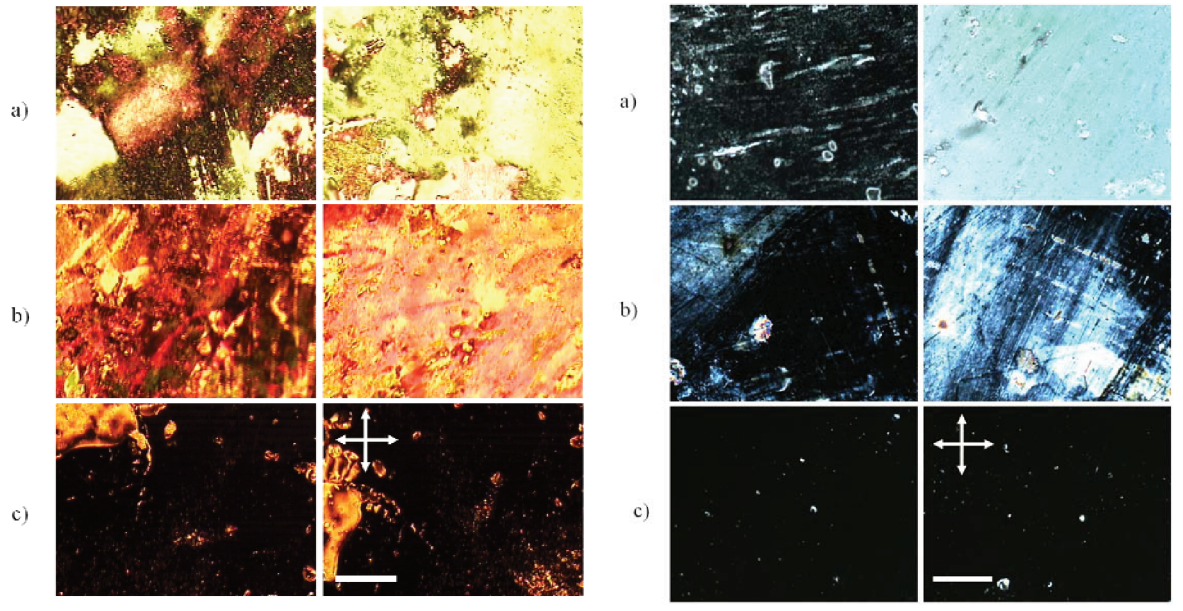

Figure 5. Polarized optical microscopy (POM) images for 5CB cells sandwiched with ILS-coated glass slides at different surface pressures. Left: Z10, (a) 3 mN/m, (b) 10 mN/m, and (c) 20 mN/m. Right: Z4, (a) 8 mN/m, (b) 21 mN/m, and (c) 33 mN/m. For each set of results, the left image represents the dark state, and the right image represents the light state (described in Experimental Methods); the rotation between these images is 45° counter-clockwise. The crossed arrows indicate the direction of the polarizer and analyzer, and the bar is 200 μm.

central core to the end acid group rises higher above the water for Z10 than for Z4 (note that the length of this chain is the only difference between Z10 and Z4). These results reinforce the idea that the acid group is the segment of the molecule most strongly tethered to the water surface and that a longer tether is floppier. However, for the infinite dilution case, there is not much of a structural difference between Z10 and Z4.

The results are more interesting for high concentrations, when packed monolayers of Z10 and Z4 are compared. The distributions of the vertical positions of various parts of the molecule are

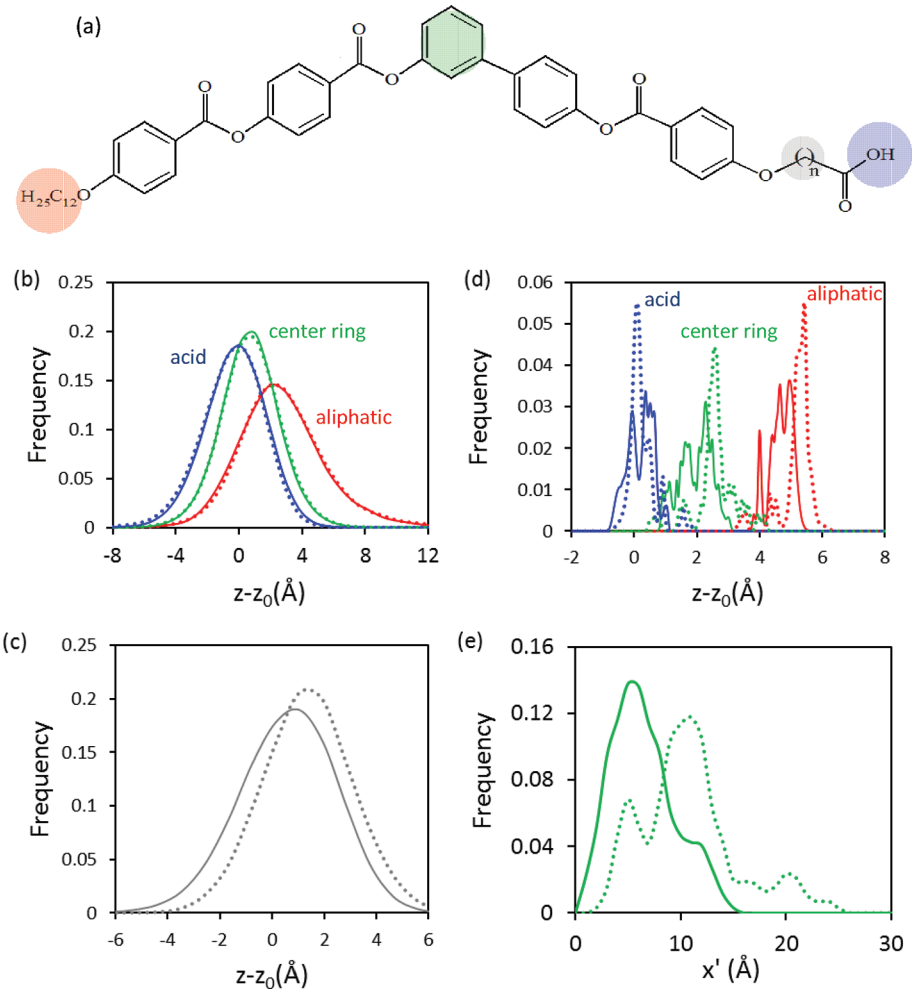

Figure 6. Distribution of the positions of the molecule segments (a). Blue represents the acid group, green represents the center ring, red represents the aliphatic end of the molecule, and gray (c) represents the center of the tether. Dotted lines represent results for Z10, and solid lines represent results for Z4. (b,c) Dilute concentration, z-coordinate relative to the water surface. (d) High concentration, z-coordinate relative to the water surface. (e) High concentration, projected coordinate perpendicular to z-axis.

shown in Figure 6d. Again, the lowest part of the molecule is the acid end, and the highest part of the molecule is the aliphatic end, but in this case, the molecule is essentially standing upright: the most probable height of the aliphatic end is approximately 50 Å for Z10 and 45 Å for Z4 above that of the acid end. There is a broader range of positions in the high concentration case than in the low concentration case because the molecules pack in a noncrystalline (disordered) way so that each of the 25 molecules in the simulation is in a somewhat disordered environment. While the above results addressed the vertical positions of molecular segments, we quantify the lateral positions (perpedicular to z) of the molecular segments by x'_i, which represents the distance of molecular segment i along the end-to-end vector of the molecule in the directions perpendicular to z and is obtained as

$$\langle x'_i \rangle = \left\langle \frac{r_{1i,x} r_{1N,x} + r_{1i,y} r_{1N,y}}{\sqrt{(r_{1N,x})^2 + (r_{1N,y})^2}} \right\rangle$$

where $r_{1i,\alpha}$ is the α component of the vector from the first to the i^{th} segment, $r_{1N,\alpha}$ is the α component of the end-to-end vector, and the $\langle ... \rangle$ represent an average over time. The results for x' of the central phenyl ring are shown in Figure 6e; this distribution is significantly broader for Z10 than for Z4, indicating that there are signifcantly larger lateral fluctutions for Z10. Similar results are obtained for the other phenyl rings in the molecule. (We note that the distributions along the z-dimension of the central phenyl ring, shown in Figure 6d, are broader for Z4 than Z10; however, this is a small effect, as these differences involve only distances of ~2 Å, while the differences in the lateral dimensions involve distances of ~20 Å.)

These average molecular structures are more easily visualized by two-dimensional projections, as shown in Figure 7. The vertical dimensions of these projections are simply the z-coordinates of the molecule segment relative to that for the water surface. The magnitude of the fluctuations in the positions is shown by bars, which represent the standard deviation of the distribution of the positions for that segment during the simulation.

These projections show visually that at dilute concentrations the Z10 and Z4 structures are very similar but that at high concentrations the Z10 molecules have much larger lateral fluctuations. This occurs because at high concentrations the bent-core molecules stand upright, with tethers being the legs

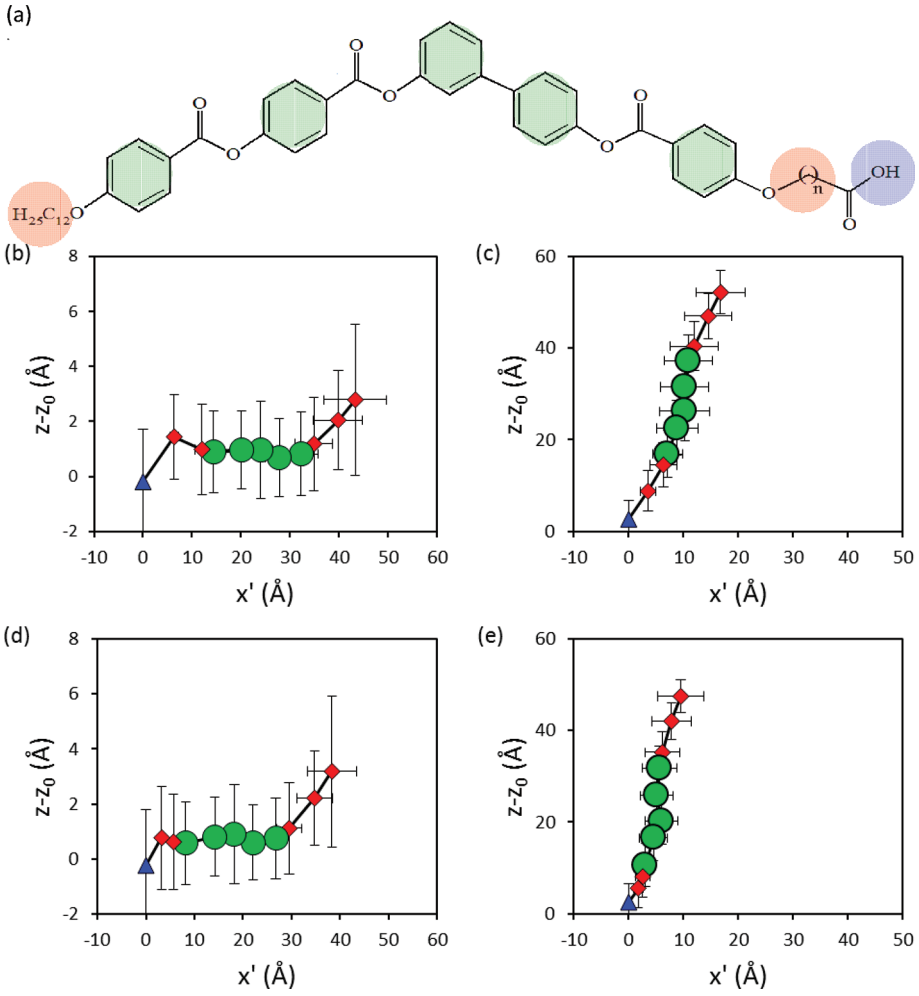

Figure 7. Two-dimensional projections of the average structures of the bent-core molecules. Green circles represent phenyl groups, red diamonds represent points along an aliphatic chain, and blue triangles represent acid groups. Bars represent the standard deviations of the width of the probability distributions for these values. Projections are shown for (b) Z10 at low concentration, (c) Z10 at high concentration, (d) Z4 at low concentration, and (e) Z4 at high concentration.

upon which they stand. Thus, a more flexible tether leads to wobbly legs, which causes large lateral fluctuations in the molecule (when it is standing upright). We believe it is these lateral fluctuations that inhibit monolayer stability.

This effect is only significant at sufficiently high concentrations such that the molecules stand upright on their wobbly legs. At low concentrations, in contrast, the molecules lie on their sides, and their wobbly legs do not have significant effects.

CONCLUSIONS

Bent-core molecules hold promise as alignment layers to orient bulk liquid crystal phases composed of other bent-core molecules. Our previous work showed that the most effective molecules for these alignment layers have a hydrophilic group that acts to tether the molecule to the water surface. Here, we compare the behavior of two molecules that differ only in their tether length and show that the length of the tether affects both the stability and organization of inverse Langmuir−Schaefer films created from these molecules and their effectiveness as alignment layers. The molecule with the shorter tether formed films with more stable isotherms and which led to more effective alignment of bulk liquid crystal phases. The floppiness of the longer tether presumably impeded the organization of the monolayers. The results of molecular dynamics simulations suggest that this occurs because at high concentrations, the molecules stand upright on the tether, and the floppier tether leads to wobbly legs that cause large lateral fluctuations in the molecular positions and reduce monolayer stability.

We also observe in the AFM images of the transferred films that while the average height deviations of films of the two molecules are similar at a given surface pressure, the horizontal scale of these deviations is strikingly different, differing by almost an order of magnitude. It would be interesting to study how the increased floppiness at molecular scales, with a mean molecular area of ~0.5 nm^2, can lead to a more gradually varying film height at scales of 500−10^4 nm^2.

ACKNOWLEDGMENT

This work was funded by NSF grants DMR-0907055 and DMR-0906852. We would like to thank the Ohio Supercomputer Center for their allocation of computing time used in this study.

REFERENCES

(1) Takezoe, H.; Takanishi, Y. *Jpn. J. Appl. Phys.* **2006**, *45*, 597–625.
(2) Araoka, F.; Sugiyama, G.; Ishikawa, K.; Takezoe, H. *Opt. Mater.* **2011**, *1*, 27–35.
(3) Pelzl, G.; Diele, S.; Weissflog, W. *Adv. Mater.* **1999**, *11*, 707–724.
(4) Jákli, A.; Krüerke, D.; Nair, D. G. *Phys. Rev. E: Stat., Nonlinear, Soft Matter Phys.* **2003**, *67*, 051702.
(5) Verduzco, R.; Luchette, P.; Hong, S. H.; Harden, J.; DiMasi, E.; Palffy-Muhoray, P.; Kilbey, S. M., II; Sprunt, S.; Gleeson, J. T.; Jákli, A. *J. Mater. Chem.* **2010**, *20*, 8488–8495.
(6) Link, D. R.; Natale, G.; Shao, R.; Maclennan, J. E.; Clark, N. A.; Körblova, E.; Walba, D. M. *Science* **1997**, *278*, 1924–1927.
(7) Niori, T.; Sekine, T.; Watanabe, J.; Furukawa, T.; Takezoe, H. *J. Mater. Chem.* **1996**, *6*, 1231.
(8) Sekine, T.; Niori, T.; Sone, M.; Watanabe, J.; Choi, S. W.; Takanishi, Y.; Takezoe, H. *Jpn. J. Appl. Phys.* **1997**, *36*, 6455–6463.
(9) Mann, E. K.; Iglesias, W.; Smith, T.; Basnet, P.; Lacks, D. J.; Jákli, A. *Emerging Liquid Crystal Technologies VI*, SPIE Proceedings, San Francisco, CA, Jan 22−27, 2011; paper no. 7955−17
(10) Iglesias, W.; Smith, T. J.; Basnet, P. B.; Stefanovic, S. R.; Tschierske, C.; Lacks, D. J.; Jákli, A.; Mann, E. K. *Soft Matter* **2011**, *7*, 9043–9050.
(11) Wang, J.; Qiu, L.; Jákli, A.; Weissflog, W.; Mann., E. K. *Liq. Cryst.* **2010**, *37*, 1229–1236.
(12) Kinoshita, Y.; Park, B.; Takezoe, H.; Niori, T.; Watanabe, J. *Langmuir* **1998**, *14*, 6256–6260.
(13) Ashwell, G. J.; Amiri, M. A. *J. Mater. Chem.* **2002**, *10*, 2181.
(14) Baldwin, J. W.; Amaresh, R. R.; Peterson, I. R.; Shumate, W. J.; Cava, M. P.; Amiri, M. A.; Hamilton, R.; Ashwell, G. J.; Metzger, R. M. *J. Phys. Chem. B* **2002**, *106*, 12158.
(15) Zou, L.; Wang, J.; Beleva, V. J.; Kooijman, E.; Primak, S. V.; Risse, J.; Weissflog, W.; Jákli, A.; Mann, E. K. *Langmuir* **2004**, *20*, 2772.
(16) Blinov, L. M.; Geivandov, A. R.; Lazarev, V. V.; Palto, S. P.; Yudin, S. G.; Pelzl, G.; Weissflog, W. *Appl. Phys. Lett.* **2005**, *87*, 241913.
(17) Blinov, L. M.; Palto, P.; Lazarev, V. B.; Geivandov, A. R.; Yuding, S. G. *Crystallogr.* **2006**, *51*, 843–849.
(18) Geivandov, A. R.; Alto, S. P.; Yudin, S. G.; Blinov, L. M.; Pelzl, G.; Weissflog, W. *Ferroelectrics* **2006**, *344*, 247–254.
(19) Wang, J.; Zou, L.; Weissflog, W.; Jákli, A.; Mann, E. K. *Langmuir* **2006**, *22*, 3198–3206.
(20) Duff, N.; Wang, J.; Mann, E. K.; Lacks, D. J. *Langmuir* **2006**, *22*, 9082–9085.
(21) Duff, N.; Mann, E. K.; Lacks, D. J. *Langmuir* **2008**, *24*, 4456–4460.
(22) Kardas, D.; Prehm, M.; Baumeister, U.; Pocienta, D.; Reddy, R. A.; Mehl, G. H.; Tschierske, C. *J. Mater. Chem.* **2005**, *15*, 1722–1733.
(23) Fang, F. Y.; Gehlert, U.; Shashidar, R.; C. M. Knobler, C. M. *Langmuir* **1999**, *15*, 297.
(24) Jorgensen, W.; Maxwell, D.; Tirado-Rives, J. *J. Am. Chem. Soc.* **1996**, *118*, 11225.
(25) Charifson, P.; Hiskey, R.; Pedersen, L. *J. Comput. Chem.* **1990**, *11*, 1181.
(26) Ryckaert, J.; Bellemans, A. *Chem. Phys. Lett.* **1975**, *30*, 123.
(27) Karpfen, A.; Choi, C.; Kertesz, M. *J. Phys. Chem.* **1997**, *101*, 7426.
(28) Wang, J.; Kallnichev, A. G.; Kirkpatrick, R. J. *J. Phys. Chem.* **2009**, *113*, 11077–11085.
(29) Darden, T.; Perera, L.; Li, L.; Pedersen, L. *Structure* **1999**, *7*, R55–R60.
(30) Bussi, G.; Parrinello, M. *Comput. Phys. Commun.* **2008**, *179*, 26.
(31) Hess, B.; Kutzner, C.; van der Spoel, D.; Lindhal, E. *J. Chem. Theory Comput.* **2008**, *4*, 435–447.
(32) Basnet, P. Patterns and Conformations in Molecularly Thin Films. Ph.D. Dissertation, Kent State University, 2010.
(33) Latterini, L.; Blossey, R.; Hofkens, J.; Vanoppen, P.; De Schryver, F. C.; Rowan, A. E.; Nolte, R. J. M. *Langmuir* **1999**, *15*, 3582–3588.
(34) Cheyne, R. B.; Moffitt, M. G. *Langmuir* **2005**, *21*, 5453–5460.
(35) Liu, L.; Kim, J.-K.; Gunawidjaja, R.; Tsukruk, V. V.; Lee, M. *Langmuir* **2008**, *24*, 12340–12346.
(36) Liu, L.; Kim, H. J.; Lee, M. *Soft Matter* **2011**, *7*, 91–95.